Enabling 3D Ambient Light Positioning with Mobile Phones and Battery-Free Chips

Lingkun Li, Pengjin Xie, and Jiliang Wang, *Member, IEEE*

Abstract—Visible Light Positioning (VLP) has attracted much research effort recently. Most existing VLP approaches require special designed light or receiver, collecting light information or strict user operation (e.g., horizontally holding the mobile phone). This incurs a high deployment, maintenance and usage cost. We present RainbowLight, a low-cost ambient light 3D localization approach that is easy to deploy in today's buildings. Our key finding is that light through a chip of polarizer and birefringence material produces specific interference and light spectrum at different directions to the chip. We derive a model to characterize the relation for direction, light interference, and spectrum. Exploiting the model, RainbowLight calculates the direction to a chip after taking a photo containing the chip. With multiple chips, RainbowLight designs a direction intersection based method to derive the location. We implement RainbowLight and extensively evaluate its performance in various environments. The evaluation results show that RainbowLight achieves an average localization error of 3.3 cm in 2D and 9.6 cm in 3D for light on, and an error of 7.4 cm in 2D and 20.5 cm in 3D for light off scenario in the daytime.

Index Terms—Visible light positioning, indoor localization

1 Introduction

The rapid development of mobile and Internet of Things (IoTs) facilitates the development of a smarter world. More and more smart robots and smart devices are used in different places, such as factories, airports and even at home. Indoor localization significantly expands the capability of these devices, and thus it attracts much research effort, e.g., a large collection of RF-based [1], [2], [3], [4], [5], [6] positioning approaches are proposed.

Visible Light Positioning (VLP) has recently been shown as a promising approach for indoor localization, owing to its potential of high localization precision with ubiquitous existence of light. The basic idea of VLP is to exploit features and information from received light to derive the relative position to light. For example, many approaches use LED light with a controller [7], [8], [9], [10], [11] to modulate the required features. Thus a receiver can use the modulated features for localization. Further, instead of using a controller to actively modulate information in light, many approaches [12], [13], [14], [15] resort to using intrinsic features of light or receiver. Meanwhile, [16], [17], [18], [19], [20], [21] use geometrical relationships among lights for localization.

Existing VLP approaches exhibit high accuracy for indoor localization. However, there still exist the following limitations that hinder their application: (1) Special designed LEDs with controllers [7], [11] or the receiver with sensors [10], [21]. Such kinds of LED/receiver are still not widely used in today's buildings. (2) Pre-collected features for all lights[13], [14]. This introduces a high overhead. It is difficult to ensure the features are stable over time and the system needs to keep updated with all lights. (3) Strict usage requirement. For example, [13] requires to keep the mobile phone horizontal and [16] requires to capture at least 3 lamps in a photo each time. (4) Do not work when the light is turned off in the daytime. During the daytime, people often turn their lights off and use the ambient light, i.e., sunlight passing through the window, to meet the requirement of illumination. Like DarkLight [22] in the field of visible light communication (VLC) realizes the requirement of communication with extremely-low luminance, we think that perform localization with the light turned off is non-trivial as well. Existing works could not work at all when the light is switched off because they are depended on LEDs or receivers. Those limitations incur a high deployment, maintenance and usage overhead.

To address those limitations, we propose RainbowLight, a low-cost 3D localization approach which significantly reduces the deployment, maintenance, and usage overhead. Our key finding for RainbowLight is that light through a chip containing polarizer and birefringence material will produce different interference patterns and light spectrum in different directions. We go deep into the birefringence principle to analyze the relationship between direction, light interference, and spectrum and derive a model to characterize the relationship. The model builds the foundation of obtaining the direction to a chip based on the received light spectrum. By calculating directions to multiple chips, we can derive the 3D localization of the receiver theoretically.

In the practical design of RainbowLight, we find that the light spectrum is difficult to measure on commercial off-

- *L. Li is with the Department of Computer Science and Engineering, Michigan State University, East Lansing, MI 48823 USA. E-mail: lilingk1@msu.edu.*
- *P. Xie and J. Wang are with the School of Software and BNRist, Tsinghua University, Beijing 100084, P.R. China. E-mail: xpj15@mails.tsinghua.edu.cn, jiliangwang@tsinghua.edu.cn.*

Manuscript received 25 Mar. 2019; revised 10 Sept. 2019; accepted 10 Nov. 2019. Date of publication 26 Nov. 2019; date of current version 3 Feb. 2021. (Corresponding author: Jiliang Wang.)
Digital Object Identifier no. 10.1109/TMC.2019.2956128

the-shelf (COTS) mobile phones. We use the color extracted from photo to approximate light spectrum and show its effectiveness. To derive light direction for localization, the theoretical model requires various parameters, e.g., optic parameters and thickness of the material, which are difficult to measure in practice. Instead of measuring those parameters, we build a sparse initial mapping between hue value and direction by sampling. Further, we conduct model-based interpolation on the sparse initial mapping to derive a fine-grained mapping. Such a sparse sampling only needs to be performed once for the same type of polarizer and birefringence material. After capturing a photo containing multiple chips, we extract the color pattern of those chips and calculate directions to them. Finally, we leverage a direction based intersection method to calculate the location.

In our implementation, we use transparent adhesive tape as birefringence material. We make small transparent chips by sticking tape with a thin plastic polarizer. In localization, we only need to place multiple chips to a certain plane (e.g., lamp cover, a glass window) to enable it for 3D localization (see Fig. 8). It should be noted that RainbowLight does not actively modulate information in the light, and thus it also works for light off scenario in the daytime. We can place chips on a wall, table, or other flat surfaces. This significantly extends the application scenarios.

We evaluate the performance of RainbowLight in different scenarios for different types of light as well as different types of surfaces. The evaluation results show that RainbowLight achieves a high localization accuracy and low cost. It also works well even for light off scenario in the daytime.

The contributions of our work are as follows:

- We show that light through a chip made by polarizer and birefringence material will produce different interference patterns and light spectrum in different directions. We analyze and derive a model to characterize the direction, interference, and light spectrum as the foundation for 3D localization.
- Based on the model, we propose RainbowLight, a low-cost ambient light 3D localization approach with a low deployment, maintenance, and usage cost.
- We implement RainbowLight and evaluate its performance through extensive experiments. RainbowLight achieves an average localization error of 3.3 cm in 2D and 9.6 cm in 3D, and an error of 7.4 cm in 2D and 20.5 cm in 3D for light off scenario in the daytime.

The organization of the remainder is as follows. Section 2 introduces the background of our work. Section 3 presents 3D localization model of RainbowLight. Sections 4 and 5 introduce the design and implementation of RainbowLight, respectively. Section 6 discusses the approach of deploying RainbowLight to enable getting the absolute position in a large area. Section 7 presents evaluation results of RainbowLight. Section 8 introduces related work and Section 9 concludes this work.

2 Background

2.1 Polarization

Polarization is a feature of the transverse wave to specify its oscillation in different directions. Natural light, such as light from a lamp, has different oscillations. Polarizer for light is a kind of device that allows light with the oscillation direction parallel to its *transmission axis*, and blocks light with the oscillation direction perpendicular to its transmission axis. The polarizer is widely used in various applications, e.g., each 3D glasses has two polarizers for two lenses with different transmission axes allowing light with different oscillation to pass.

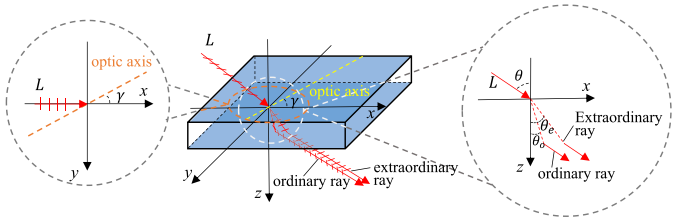

Fig. 1. Illustration of birefringence.

A polarizer with a single transmission axis is called *linear polarizer*. Light is polarized after passing through a polarizer. The polarized light has an oscillation direction parallel with the transmission axis of the polarizer. Denote the angle between the oscillation direction of light and the transmission axis of a polarizer as ϕ, according to Malus's law [23], the intensity of the light that passes through the polarizer, denoted by I_ϕ, is given by

$$I_\phi = Icos^2\phi, \tag{1}$$

where I is the original intensity of light.

Natural light has oscillation in any direction. When natural light passes through a linear polarizer, it becomes linearly polarized light, i.e., light with a single oscillation direction.

2.2 Birefringence

Birefringence [24] is a feature for an optically anisotropic material such as plastics, calcite, and quartz. When a ray of light passes through a birefringence material, two refracted rays can be observed. As shown in Fig. 1, the ray of light is split into two rays taking different paths in the material. Meanwhile, those two rays have orthogonal polarization directions and different refractive indices in the birefringence material. There is a special direction, namely *optic axis*, for each certain type of birefringence material. One of the two rays, called *ordinary ray*, has a polarization direction vertical with the optic axis. Its refractive index is called *ordinary refractive index* and is denoted by n_o. Another ray, called *extraordinary ray*, has a polarization direction along the optic axis. Its refractive index is called *extraordinary refractive index* and is denoted by n_e.

As shown in Fig. 1, according to Snell's Law [25], we have

$$n_{air}sin\theta = n_esin\theta_e = n_osin\theta_o, \tag{2}$$

where $n_{air} \approx 1$ is the refractive index in air, and θ_o and θ_e are the refractive angle of ordinary ray and extraordinary ray, respectively. Usually, $n_e \neq n_o$, and the refractive angles and refractive indexes of ordinary ray and extraordinary ray are different. Thus there is an optical path difference between the two rays after the birefringence material. For a certain type of material, n_o is fixed determined by the material, while n_e varies depending on the direction of the incident

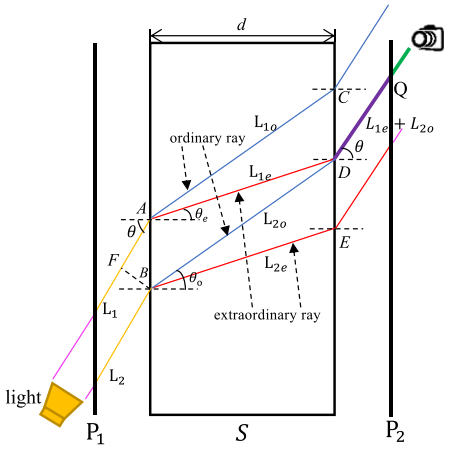

Fig. 2. Illustration of light interference.

ray. As shown in Fig. 1, denote the incident angle as θ and the angle between the incident light projection on the incident plane and optic axis as γ. We will show how to obtain n_e and θ_e using θ and γ in practice. Then we can calculate the optical path for ordinary ray and extraordinary ray.

According to Snell's Law, if the incident light L is linearly polarized and the angle between polarization direction and optic axis is ϕ_1, the intensity of ordinary ray I_o and extraordinary ray I_e can be calculated as

$$\begin{aligned} I_o &= I\sin^2\phi_1 \\ I_e &= I\cos^2\phi_1, \end{aligned} \tag{3}$$

where I is the intensity of L.

2.3 Interference

When two light beams L_1 and L_2 have the same frequency, stable phase difference δ and same polarization direction, they can interfere with each other. For a different value of δ, the two light beams can have different interference results. The interference intensity can be calculated as:

$$I_i = I_1 + I_2 + 2\sqrt{I_1 I_2}cos\delta, \tag{4}$$

where I_i is the light intensity after interference, and I_1 and I_2 are the intensities of L_1 and L_2, and δ is the phase difference between L_1 and L_2 and often derived from the optical path difference.

3 Localization Basics

We aim to answer the question of why observing the chip made by polarizers and birefringence material in different directions would get different color patterns. In this section, we first build a model from the background to show the principle of our 3D positioning approach. Then we conduct an experiment to validate our model. Because some of the parameters are hard to measure, it is difficult to directly use such a model to perform positioning directly. As a result, we show how to address those challenges in our design in Section 4. Therefore, readers who are not interested in the detailed analysis of RainbowLight can skip this section directly.

As shown in Fig. 2, a birefringence material S is placed between two polarizers P_1 and P_2. Light from a source (e.g., a lamp) first passes through polarizer P_1 and becomes a linearly polarized light. Consider two rays of the polarized light L_1 and L_2 incident into S at point A and B, respectively. As introduced in Section 2, L_1 is separated into two parts: L_{1o} (the ordinary ray) and L_{1e} (the extraordinary ray). The refractive indices of the ordinary ray and the extraordinary ray are n_o and n_e, respectively. Similarly, L_2 is separated into two parts: L_{2o} (the ordinary ray) and L_{2e} (the extraordinary ray). After passing through another polarizer P_2, the light L_{1e} and L_{2o} become L'_{1e} and L'_{2o}. L'_{2o} of L_2 interferes with L'_{1e} of L_1. Then the interference result of light L'_{2o} and L'_{1e} is measured by a camera at Q.

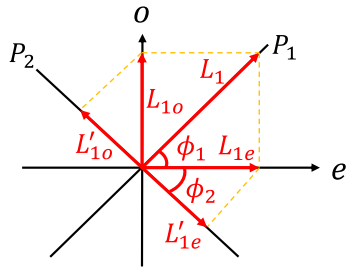

Fig. 3. Polarization and intensity change through P_1, S and P_2.

Next, in this section, we analyze the light spectrum of interference results and show its relationship with the angle θ.

3.1 Interference Analysis

From Eq. (4), we can know that the interference light intensity relies on the two coherent light intensity and their phase difference. We analyze the intensity and phase difference of L'_{1e} and L'_{2o} in the following part.

3.1.1 Intensity

Assume the angles between the optic axis of S and the transmission axes of two polarizers P_1 and P_2 are ϕ_1 and ϕ_2, respectively. As shown in Fig. 3, L_1 is the result of light after passing through P_1 and thus its polarization direction is parallel with the transmission axis of P_1. Denote the intensity of L_1 as I_1, and assume light ray L_1 and L_2 have equal intensity. According to Eq. (3), $I_{1o} = I_1\sin^2\phi_1$ and $I_{1e} = I_1\cos^2\phi_1$.

Denote the light intensities of L'_{1e} and L'_{2o} as I'_{1e} and I'_{2o}, respectively. According to Eq. (1), I'_{1e} and I'_{2o} can be calculated as

$$\begin{aligned} I'_{2o} &= I_{1o}sin^2\phi_2 = I_1 sin^2\phi_1 sin^2\phi_2 \\ I'_{1e} &= I_{1e}cos^2\phi_2 = I_1 cos^2\phi_1 cos^2\phi_2. \end{aligned} \tag{5}$$

3.1.2 Phase Difference

As shown in Fig. 2, the incident angles of L_1 and L_2 to S are both θ, the thickness of S is d, and the refraction angles of L_{1e} and L_{2o} are θ_e and θ_o. The optical path difference Δ of L_{1e} and L_{2o} at point Q can be calculated as

$$\begin{aligned} \Delta &= \overline{FA}n_{air} + \overline{AD}n_e - \overline{BD}n_o \\ &= d(tan\theta_o - tan\theta_e)(sin\theta)n_{air} + \frac{d}{cos\theta_e}n_e - \frac{d}{cos\theta_o}n_o, \end{aligned} \tag{6}$$

where $\overline{FA}$, $\overline{AD}$, and $\overline{BD}$ are the lengths from F to A, from A to D, and from B to D, respectively.

Combining Eqs. (2) and (6), we have

$$\Delta = d(n_e cos\theta_e - n_o cos\theta_o). \tag{7}$$

As aforementioned, for a particular material, n_o is usually fixed, n_e and θ_e are related to the incident angle. We put the details of calculating n_e, θ_e and Δ in Section 3.1.3. Therefore, we have

$$\Delta = d(\sqrt{N_e^2 - sin^2\theta(sin^2\gamma + \frac{N_e^2}{N_o^2}cos^2\gamma)} - \sqrt{N_o^2 - sin^2\theta}), \tag{8}$$

where N_o and N_e are principal refractive indices of S, which are fixed given a certain type of material, θ is the incident angle, and γ is the angle between the projection of incident light on the incident plane and optic axis, which is shown in Fig. 1.

The optical path difference is for two light beams, the phase difference is different for different wavelength. For light with a specific wavelength λ, we can calculate the phase difference δ of L_{1e} and L_{2o} at point D as

$$\delta_D = \Delta\frac{2\pi}{\lambda}. \tag{9}$$

Due to the phase difference of projection on P_2, the phase difference between two coherent lights L'_{1e} and L'_{2o} at point Q is

$$\begin{aligned}\delta &= \delta_D + \delta' \\ &= \begin{cases} \Delta\frac{2\pi}{\lambda} & (\text{case } 1) \\ \Delta\frac{2\pi}{\lambda} + \pi & (\text{case } 2) \end{cases},\end{aligned} \tag{10}$$

where case 1 means the vectors L'_{1o} and L'_{1e} are in the same direction on P_2, and case 2 means they have reverse directions.

3.1.3 Calculation of n_e, θ_e, and Δ

Inspired by [26], as shown in Fig. 1, the directional vector of optical axis, ordinary ray, and extraordinary ray in the birefringence are

$$e_a = (cos\gamma, sin\gamma, 0) \tag{11}$$

$$e_{ko} = (sin\theta_o, 0, cos\theta_o) \tag{12}$$

$$e_{ke} = (sin\theta_e, 0, cos\theta_e). \tag{13}$$

We assume the angle between optic axis and extraordinary ray is α, i.e., angle between e_a and e_{ke}. So according to Eqs. (11), (13), we have:

$$cos\alpha = e_a \cdot e_{ke} = cos\gamma sin\theta_e. \tag{14}$$

Because the refractive index of extraordinary ray varies with different incident angles, according to the relationship between α and the refractive index of extraordinary ray n_e in [27], we have

$$n_e = \frac{N_o N_e}{\sqrt{N_o^2 sin^2\alpha + N_e^2 cos^2\alpha}} = \frac{N_o N_e}{\sqrt{N_o^2 + (N_e^2 - N_o^2)cos^2\alpha}}. \tag{15}$$

where N_o and N_e are principal refractive indices and are fixed for each type of material. According to Eqs. (14), (15), we have:

$$n_e = \frac{N_o N_e}{\sqrt{N_o^2 + (N_e^2 - N_o^2)cos^2\gamma sin^2\theta_e}}. \tag{16}$$

According to Snell's Law, we have:

$$n_{air} sin\theta = n_e sin\theta_e = n_o sin\theta_o. \tag{17}$$

where $n_{air} \approx 1$ is the refractive index in air. Then we have

$$n_e = \frac{sin\theta}{sin\theta_e}. \tag{18}$$

According to (16), (18), we have:

$$\theta_e = \arcsin\sqrt{\frac{sin^2\theta}{N_e^2 - sin^2\theta\left(\frac{N_e^2}{N_o^2}cos^2\gamma - cos^2\gamma\right)}}. \tag{19}$$

Finally, according to Eqs. (18) and (19), we have:

$$n_e = \sqrt{N_e^2 - sin^2\theta\left(\frac{N_e^2}{N_o^2}cos^2\gamma - cos^2\gamma\right)}. \tag{20}$$

Because the optical path difference is

$$\Delta = d(n_e cos\theta_e - n_o cos\theta_o). \tag{21}$$

We substitute n_e, θ_e, and n_o, θ_o into Eq. (21), we can have the expression of Δ using known parameters

$$\Delta = d(\sqrt{N_e^2 - sin^2\theta(sin^2\gamma + \frac{N_e^2}{N_o^2}cos^2\gamma)} - \sqrt{N_o^2 - sin^2\theta}). \tag{22}$$

3.1.4 Summary

According to Eq. (4), the intensity spectrum of the interference light at Q can be calculated as

$$\begin{aligned}I_Q =& I_1 cos^2\phi_1 cos^2\phi_2 + I_1 sin^2\phi_1 sin^2\phi_2 \\ &+ 2I_1 cos\phi_1 cos\phi_2 sin\phi_1 sin\phi_2 cos\delta.\end{aligned} \tag{23}$$

where δ can be calculated according to Eq. (10).

According to Eq. (23), given the intensity spectrum on frequency domain of light source I_1, the angle ϕ_1 between optic axis of the birefringence material and the polarizer P_1, the angle ϕ_2 between optic axis of the birefringence material and the polarizer P_2, the incident direction parameters θ and γ, and birefringence material parameters principal refractive indices and thickness d, we can calculate the value of the light intensity I_Q at Q.

Fig. 4 shows the light spectrum of interference for different parameters. Given the value of I_1, ϕ_1, ϕ_2 and d, different combinations of θ and γ result in different spectrum of I_Q.

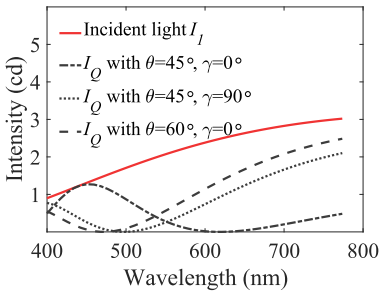

Fig. 4. Intensity of interference light for different wavelength with different incident angles.

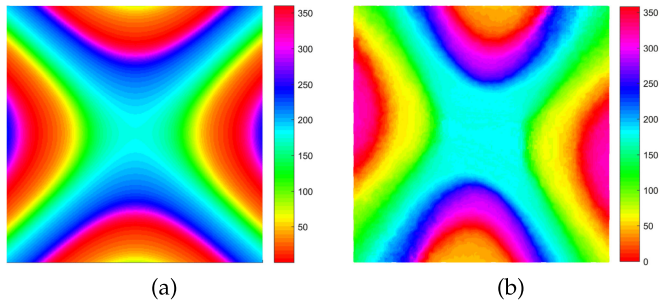

Fig. 5. (a) Hue values on x-y plane by simulation. (b) Hue values measured by mobile phone on x-y plane.

This makes the foundation of obtaining light incident angles based on different interference results. As long as we can get the incident angles from multiple points, we can use the AoA-based method for localization.

3.2 Validation

3.2.1 Choose the Light Spectrum Feature

Mobile cameras usually do not have the capability of measuring the light spectrum directly. However, the direction is represented by the interference light spectrum, and we have to distinguish different light spectrums to distinguish different directions. There is a challenge for us to find a proper light feature, which satisfies two conditions in the meantime: it can be measured by the COTS camera and can indicate the direction from the source to the chip. It is well-known that different light spectrums result in different colors of the mixed light. A straightforward approach is to measure the RGB color and map RGB vectors to different directions. However, we find this is not feasible in practice as the spectrum could not be effectively represented in RGB color. Instead, we use the Hue, Saturation, Lightness (HSL) color space and find that the H (i.e., Hue) component from HSL is much more suitable for representing the color of mixtures of lights [28].

3.2.2 Measurement Result

We conduct an experiment to validate the model. We measure the hue value on different positions after P_2. Fig. 5b shows the measurement hue values for different positions on a plane with a certain distance to the light source. Then we compare the measurement result with the simulation result based on Eq. (23). In our simulation, we use the parameters of quartz crystal (a type of birefringence material) chip with thickness of 0.6 mm. We measure the intensity spectrum of interference result on different direction. We leverage the color wheel [28] to approximate intensity spectrum with hue value. Fig. 5a shows the hue value with respect to positions on a surface parallel with the birefringence chip. We can see that the color regularities of Figs. 5a and 5b are very similar. This coincides with our analysis and Eq. (23). This also means that hue value is effective for representing the intensity spectrum.

4 RainbowLight Design

4.1 Design Overview

Fig. 6 illustrates the system overview of RainbowLight. The chips used in RainbowLight are a combination of two polarizers and one birefringence chip as shown in Fig. 2. With one chip, we can calculate direction information. Combining the direction information from multiple chips, we can derive the 3D location. The main design of RainbowLight consists of two parts. The first part is mapping initialization. This part is to build an initial mapping between the direction and hue value for a certain type of chip. The mapping initialization only needs to be performed once for a certain type of chip. The second part is the 3D localization component. In this part, a mobile camera will take a photo containing multiple chips. Based on the hue value of the initial mapping, the direction to those chips can be calculated. Then we also propose a direction intersection based method to calculate the final 3D location.

4.2 Mapping Initialization

The mapping between light directions and hue values can be built by sampling in different positions. We put a chip at the origin O of the coordinate system, and the chip is parallel with the x-y plane. A mobile phone moves in a grid at a certain plane ($z = 1m$) and captures a photo containing the chip at each position. For a sampling position r, it derives the hue value h of the color for the chip from the captured photo. It means that the hue values for all points on the ray $\overrightarrow{Or}$, i.e., the ray with the direction from the chip to the position on the plane in the space, are h.

Therefore, we build a map $R_S \rightarrow H_S$ from sampling positions $R_S = (r_1, r_2, \ldots, r_n)$ to hue values

$$H_S = (\, h_1, h_2, \ldots, h_n \,), \tag{24}$$

where h_i denotes the hue value observed by mobile phone from points on line $\overrightarrow{Or_i}$.

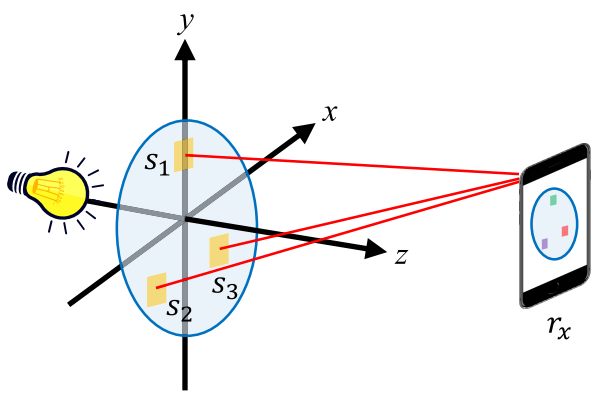

Fig. 6. Overview of RainbowLight.

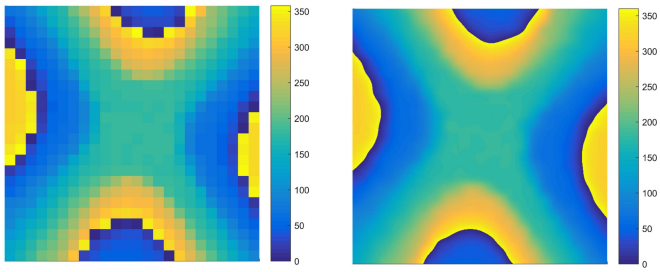

Fig. 7. Interpolation of Hue matrix. (a) coarse-sampled matrix, (b) interpolation result.

For a higher sampling density, the map should be more accurate. On the other hand, a higher density also indicates a higher sampling overhead. To reduce the initial sampling overhead, we propose an interpolation-based method to improve the granularity of initial map. We leverage the color regularity to interpolate a coarse-grained sampling matrix H_S and build a fine-grained map $R \rightarrow H$. We examine the performance of interpolation under different sampling density in Section 7.3.

As shown in Fig. 5, the color gradually changes with the position. As the hue value ranges from 0 to 360, in interpolation we should carefully deal with the hue value cross the hue range boundary. More specifically, for two hue values h_1 and h_2 ($h_1 > h_2$) for two adjacent sampling positions, we first calculate the hue value gap $h_\Delta = h_1 - h_2$. If h_Δ is smaller than a pre-defined threshold thr (e.g., $thr = 350$), the interpolation can be performed between h_1 and h_2. If h_Δ is larger than the pre-defined threshold thr, we consider the hue value between those two sampling positions crosses the hue value boundary. The interpolated hue value should be performed for h_1 and $h_2 + 360$. All the hue value should be calculated from the interpolation result modulo by 360 to guarantee the hue values are in $[0, 360)$. Fig. 7a shows the original hue matrix. Fig. 7b shows the interpolation result.

In practice for the same type of chip, we only need to build the initial map $R \rightarrow H$ once. This could significantly reduce the initialization overhead for RainbowLight. Later, we will show how to leverage the map for localization in 3D space.

4.3 3D Localization

4.3.1 Localization Design

To enable 3D localization, we simply stick several chips on a transparent surface. Without loss of generality, we assume three chips S_1, S_2 and S_3 are used. Later, in Section 7, we will show the impact of number of chips. Denote the position of the center of S_1, S_2, and S_3 as p_1, p_2 and p_3, respectively. The position p_1, p_2 and p_3, namely reference points, can be measured in advance.

A mobile phone with a camera at the position r_x simply captures a photo containing S_1, S_2, and S_3. We calculate the hue values $\tilde{h}_1$, $\tilde{h}_2$ and $\tilde{h}_3$ from the photo for those three chips. Based on the initial map between colors and directions, RainbowLight can obtain the possible directions from p_1, p_2 and p_3, respectively. Thus we have three groups of ray directions from three reference points, respectively. Then we can obtain the position r_x based on the intersection of those ray directions.

4.3.2 Intersection Based Localization

The goal of localization is to calculate the position r_x based on $\tilde{h}_1$, $\tilde{h}_2$ and $\tilde{h}_3$ and $R \rightarrow H$.

Find Line Group Candidates. The initial map is built using a chip at coordinate origin O. In practical, chips are usually attached at other positions. In order to make the map $R \rightarrow H$ suitable for the deployment of a specific chip, we need to do coordinate translation for the initial mapping. The map becomes $R^j \rightarrow H$ for $j = 1, 2, 3$, where $R^j = R + p_j$ is the transformed sampling position for S_j.

Due to the color error for the camera on a mobile phone, there may be multiple lines with hue close to $\tilde{h}_1$, $\tilde{h}_2$, and $\tilde{h}_3$. Meanwhile, according to Eq. (23), we also find that there are multiple combinations of θ and γ leading to the same hue value. It indicates that there may be multiple directions of the same hue value. Therefore, for each chip, we can calculate a group of lines. Overall, we obtain three groups of lines denoted by G_1, G_2, and G_3. We have $G_j = \{\overrightarrow{r_i^j p_j} || h_i - \tilde{h}_j| < \epsilon_h\}$ for $j = 1, 2, 3$ where $r_i^j \in R^j$ and ϵ_h is the maximum allowed hue error.

Line Intersection. The main idea is calculating the localization based on the intersection point of those three sets of lines G_1, G_2, and G_3 as the localization result r_x. There should exist three lines from G_1, G_2 and G_3, respectively, that intersect at point r_x. Due to hue value measurement error, those three lines may be very close to each other but not directly intersect in practice. Therefore, we could use an algorithm based on the contrary thinking. The idea is based on the principle that light travels in a straight line. As shown in Fig. 9, not without generality, suppose we want to perform localization in a 2D plane. If we put two chips, namely S_1 and S_2, at localization 0 cm and perform initialization at 100 cm, i.e. at point A we observe S_1 and S_2 and get hue values C_{A_1} and C_{A_2} respectively, and at point B we get hue values C_{B_1} and C_{B_2}, according to the principle, we will get hue values C_{B_1} and C_{A_2} at point C at 60 cm. Therefore, if we have sampled all points at 100 cm, hue values of nearly all points in the plane will be derived ideally. We regard all those hue values as 2D coordinates. After that when we capture a photo contains those two chips, we extract hue values, for example, (C_1, C_2), then we can get the final positioning result by calculating the minimum distance between (C_1, C_2) and all coordinates we derived. We can easily extend the algorithm above from 2D plane to 3D space.

5 Implementation

RainbowLight consists of two components: anchor and receiver. In this section, we present the details of those two components. We also discuss a variant of RainbowLight, which put polarizer P_2 in front of the camera to eliminate color observed by human eyes. Since RainbowLight performs relative localization for a given anchor, it needs to identify which anchor is captured by camera hence can be used in a large region. We also discuss how to provide identifiers to anchors in this section.

5.1 Anchor

The anchor of RainbowLight is composed of a group of chips. Each chip consists of two linear polarizers and a thin birefringence material chip. We stick the birefringence

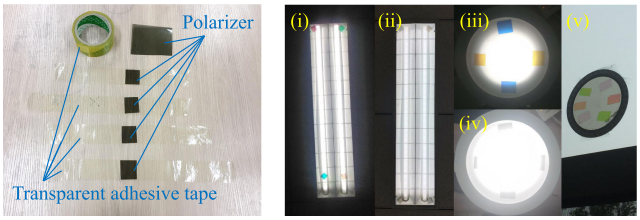

Fig. 8. (a) Chips in RainbowLight (b) anchor with chips made by two polarizers and one transparent adhesive tape (i): near to fluorescent (iii) on LED lamp cover, anchor with chips made by one polarizer and one transparent adhesive tape (ii): near to fluorescent (iv): on LED lamp cover, (v): anchor on a glass window.

material chip between two linear polarizers. As shown in Fig. 8a, we use the everyday transparent adhesive tape as the birefringence material. RainbowLight does not require to stick the anchors on a lamp. We can put anchors on different surfaces as long as light can pass through the chips. For example, as shown in Fig. 8b (i), (iii) and (v), we put anchor near lamps or on a lamp cover or a window. As shown in Fig. 8b (i) and (iii), despite chips display colors, each chip made by polarizers and transparent adhesive tape is very small. It would not disturb human eyes. To enable RainbowLight, we also need to record the relative position for those chips.

5.2 Receiver

We use the smartphone as the receiver side. The camera can capture a photo containing the anchor. We implement software on the mobile phone based on Android. While the camera is taking a photo, RainbowLight launches automatic exposure to fit the luminance of the environment. After obtaining the photo, we use the algorithm of white balance to eliminate color shift among different camera models, then use OpenCV to localize the position of each chip in the image based on features such as shapes and derive HSL information from the photo. To address hue value estimation error in practice, we use the averaged hue value for each chip as the hue value for localization. Then we use the 3D localization algorithm mentioned in Section 4.3.2 to get the position of the camera.

Now we present a variant of RainbowLight to eliminate the color which can be observed by human eyes directly. We put polarizer P_2 in front of the camera. In such a case, human eyes cannot observe the color displayed by chips directly as shown in Fig. 8b (ii) and (iv), but cameras can capture chips with different colors. However, if we put P_2 in front of the camera, the camera's rotation would result in the change of color of the chips, thus color-direction map could not be used. Fortunately, since the hue value instead of RGB represents color in

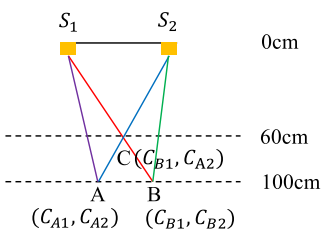

Fig. 9. Illustration of localization algorithm.

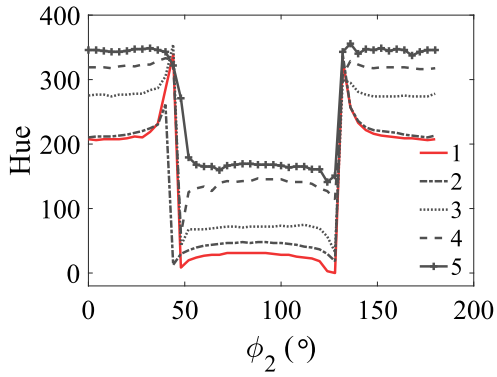

Fig. 10. Complementary hue observed as rotating mobile phone for different tape thickness (1 ~ 5).

RainbowLight, chips only show two complementary hue values with the camera's rotation as shown in Fig. 10. Therefore, we measure the camera's rotation angle first, if it results in complementary hue values of initialization, we can transform them into original hue values hence performing localization. Attaching polarizer in front of the camera will bring in extra costs, and brings error of accuracy with the camera's rotation. We will present the accuracy in Section 7. Users who deploy the RainbowLight can choose where to put the polarizer P_2 according to their conditions and requirements.

We measure the latency of RainbowLight. In the measurement, we let RainbowLight process 10 photos to measure the average latency. The mobile phone we used is Huawei Nexus 6P. It takes 236 ms on average to find chips and extract hue values. It takes 503 ms on average for 3D localization from hue values. We optimize RainbowLight 3D localization to parallel the processing in our implementation of localization. With such an optimization, the time for 3D localization reduces to 123 ms on average. This would apply to most VLP based applications such as navigation. We also use Power Monitor to measure the power consumption of RainbowLight with Nexus 5x, the result shows that our algorithm takes 1.122J to process one photo and perform localization.

6 Apply RainbowLight to Localization in a Large Area

We have presented a novel relative localization approach, RainbowLight, which can derive the camera's relative position to an anchor. However, one small RainbowLight anchor only can be captured by the camera in a small region, thus it is difficult to apply to localization in a large area such as a shopping mall. To address this issue, we can use the idea similar to use multiple lamps to illuminate an entire room, in other words, we give each anchor a unique identifier and extract the identifier from the anchor first to get a coarse-grained area where camera located, then derive precise relative location to the anchor. Therefore, we can use RainbowLight to get the camera's location in a large area.

6.1 Providing Identifier to RainbowLight Anchor

We can use the existing method such as iLAMP [14] to distinguish different light sources in a large area if we put an anchor on the lamp. We can also attach the QR code on each anchor to identify them. Considering iLAMP cannot be

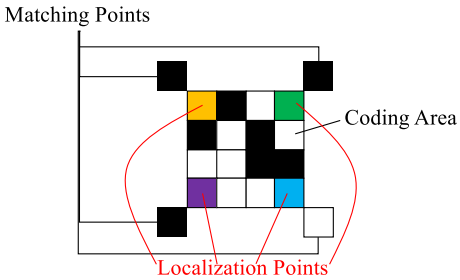

Fig. 11. RainbowLight anchor with identifier.

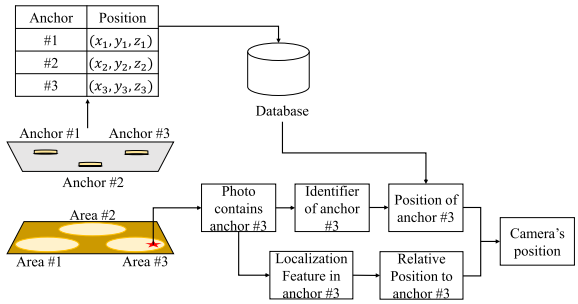

Fig. 12. Overview of localization in building.

used with light-off, we also design a QR-code-like method to use our localization chips for providing ID.

As shown in Fig. 11, after modification, an anchor consists of 3 components. While the *Localization Points* used to derive the relative position is made by polarizers and transparent adhesive tape, *Matching Points* and *Coding Area* are only made by polarizer. We make them by two perpendicular polarization directions. Similar to the QR code, 3 of matching points are in the same direction, and another is not, therefore, it can be decoded even if the anchor is rotated in the photo. We use those two directions to represent 0 or 1 in the coding area. Therefore, after taking a photo behind another polarizer either covered on the anchor or put before the camera, we can compare the brightness of each polarizer in the coding area to polarizers of matching point to recognize each of them representing 0 or 1, hence decode the identifier. In this case, the anchor can encode $2^{12} = 4096$ identifiers in the coding area.

6.2 Localization in a Large Area

As Fig. 12 shown, without loss of generality, suppose we have 3 anchors in a large area, we can store each anchor's identifier and its real position in a database in advance. During the localization process, for example, after a camera in area #3 which is a valid area of anchor #3 taking a photo containing anchor #3, the system first decodes the identifier of the anchor in the photo, then get the real position of the anchor from the database. Combining with the relative position from the camera to the anchor, we could get the camera's real position.

7 Evaluation

We evaluate the performance of RainbowLight from the following aspects:

- Localization accuracy for different distances.
- The performance of mapping the position related to the landmark to the absolute position.
- The impact of system parameters on localization accuracy.
- System performance under different light sources (different manufacturers, color temperatures, lamp types, and powers).
- System performance under different mobile phone models.
- System performance with the light on/off.
- System performance with different angles of mobile phone orientation.

Through the evaluation, we aim to show the effectiveness of RainbowLight in practice. It should be noted that for all experiments we use the same initial mapping unless otherwise specified. This means that we only need to perform initialization once, which significantly reduces the initialization overhead compared with existing approaches.

7.1 Localization Accuracy

Fig. 13a shows the experiment environment. In the experiment, we move a transparent board to different distances to the light source. For each distance, we move the mobile phone on the board at different positions. We can measure the position of the mobile phone on the board as the ground truth. Meanwhile, we also use RainbowLight to calculate the position of the mobile phone. We switch off other lamps during our experiment at night. Fig. 13b shows the localization error for the mobile phone moving on the board out of 230 random points. The x-axis denotes the range of the distance between the board and the lamp. We can see that the localization error increases as distance increases. This is mainly because hue value is less sensitive to the position for a larger distance.

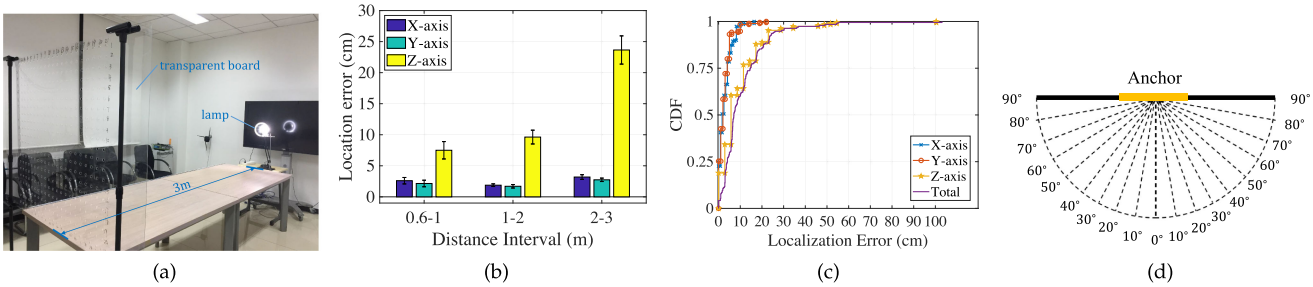

(a) (b) (c) (d)

Fig. 13. (a) Experiment environment. (b) Localization precision on different distance. (c) Localization precision map relative position to absolute position. (d) Capture in different angles.

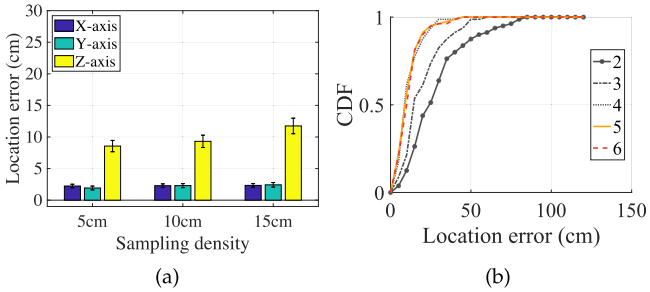

Fig. 14. Localization precision on different (a) sampling density, (b) number of chips.

We can also observe that the error on z-axis is larger than that on x-y plane. The major reason is that the angle from the chip to the mobile phone varies by a smaller value when we move the mobile phone along the z-axis than that along the x-y plane. This phenomenon is more evident when chips are close to each other. However, even when those chips are all in a circle with diameter less than 16 cm, the localization accuracy for different distance is still high. This indicates RainbowLight can work for different distance with the lamp of small size.

Overall, in the 2m - 3m distance interval, the mean error of localization is 3.19 cm on x-axis, 2.74 cm on y-axis, and 23.65 cm on z-axis. This performance is better than SmartLight with a localization error of about 60 cm on z-axis for distance from 1m - 3m. The localization accuracy of RainbowLight is enough for most of today's application scenarios such as navigation.

7.2 Performance With Identifier

As discussed in Section 6, we design an approach to map the position of a camera relative to the anchor to the absolute position in an area by providing an identifier to each anchor. To evaluate the performance of this approach, we randomly choose 190 points in an area of the meeting room, and calculate the accuracy of localization. Fig. 13c shows the performance. We can find that RainbowLight achieves 1.68 cm of the median error in the *X*-axis, 2 cm of the median error in the *Y*-axis, 5.74 cm of the median error in *Z*-axis, and 7.04 cm of the median error with the whole dimension. It also achieves 7.37cm, 5 cm, 22.9 cm, 23.20 cm of the 90 percent error in *X*-axis, *Y*-axis, *Z*-axis, and with the whole dimension, respectively. The localization accuracy is also enough for most of todays application scenarios.

To evaluate the performance of decoding of the identifier on the anchor, we use the camera to capture photos with different angles to the anchor. As shown in Fig. 13d, we put an anchor in a plane, and use the camera to capture photos from 0 to 90 degree, then try to decode the identifier on the anchor. With the identifier we designed in Section 6, it could not be decoded when the angle is above to 60 degree. Since the ceiling of a room is often with a height of 3 m, so users should deploy an anchor in every 9.42 m^2 with the code we designed in Section 6.

7.3 Impact of Sampling Density

We examine the impact of sampling density in building the initial map. Fig. 14a shows the localization accuracy with respect to different sampling densities. We build the initial map on a plane parallel to $x-y$ plane with $z = 100$ cm. We examine the performance with different inter-distance of sampling position, i.e., 5, 10, and 15 cm, respectively. It can be seen that low sampling density still works well for RainbowLight. Even when the inter-distance is 15 cm, the localization error is only around 10 cm. This is mainly because hue value distribution is smooth in the 3D space and thus interpolation is effective in building initial mapping.

7.4 Impact of Number of Transparent Chips

As shown in Section 4, the hue value from a single chip determines a candidate group of rays from the chip. With more chips, the localization accuracy will be improved as the intersection point can be refined with more groups of rays. We explore the relationship between localization accuracy and the number of chips. Fig. 14b shows the CDF of 3D localization error while increasing the number of chips from 2 to 6. It can be seen that the localization accuracy increases when the number of chips increases from 2 to 4. Further, the performance becomes relatively stable when the number increases from 4 to 6. This means 4 chips is enough in practice to achieve a good localization accuracy.

7.5 Impact of Different Light Sources

We examine the performance of RainbowLight with different light sources. As shown in Fig. 16, we use lamps of different types, i.e fluorescent (FL), LED and incandescent bulb (IL), from different manufacturers (A - E), with different color temperature (3000 K, 6000 K) and different power (5 W, 6.5 W, 12 W). In all the following experiments, we use a Philips (manufacturer A) 6.5 W LED with the color temperature of 6,000 K for initialization.

In our daily life, the power of LED mainly ranges from 5 W to 20 W. Fig. 15a shows localization error of LED (manufacturer A) of power 5 W (500 lm), 6.5 W (600 lm), and 12W (1100 lm) out of 150 random points. There is no significant difference in terms of error for different power. This is mainly because as

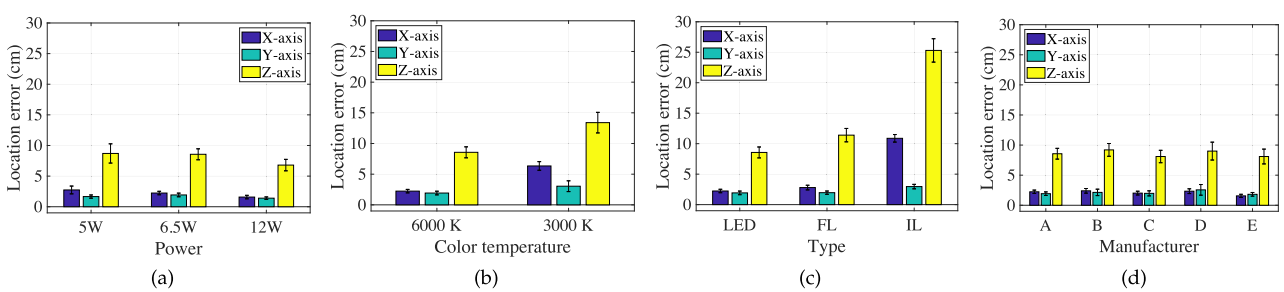

Fig. 15. Localization accuracy for different (a) power of lamp, (b) color temperature of lamp, (c) types of lamp, (d) manufacturers of lamp.

Fig. 16. Different light sources.

long as γ and θ are fixed, our approach captures the major property of light spectrum and also removes other noise such as brightness, as explained in Section 3.

There are mainly two different color temperatures (6,000 and 3,000 K) for typical lamps in our daily lives. Intuitively, 6000 K generates white color while 3,000 K generates yellow. The light spectrums from those two temperatures are slightly different. We initialize with a 6,000 K lamp and measure the localization error for 3,000 and 6,000 K out of 100 random points. As shown in Fig. 15b, we can see that the localization error of 3,000 K is slightly larger than that of 6,000 K because of spectrum difference. However, the accuracy of both color temperature is still acceptable. In practical applications, we only need to build the initial map with one color temperature, and RainbowLight performs well under other color temperatures.

We examine the performance of RainbowLight for the three most commonly used lamps, i.e., LED, fluorescent, and incandescent bulb out of 150 random points. As shown in Fig. 15c, the accuracy for fluorescent is high. The accuracy of the incandescent bulb is relatively low. This is because those two types of lamps have different light spectrums. However, as long as we use the incandescent bulb for initialization, the accuracy of RainbowLight remains high for incandescent bulb.

We also examine the performance of RainbowLight among different brands of lamps. The light spectrum emitted slightly varies for lamps from different manufacturers. We choose 5 LEDs from 5 different popular manufacturers, marked as A-E. The power of all lamps is 5 W and the lumens are 500, 380, 450, 400, and 280 lm, respectively. The color temperature is 6,000 K. Fig. 15d shows that the error is small for all brands out of 250 random points and the performance is similar for all brands. It also indicates we only need to initialize with a certain brand, and the accuracy of RainbowLight is acceptable under other brands.

Summary. RainbowLight achieves a high accuracy under different circumstances with commonly used lamps. For most scenarios, RainbowLight only needs to be initialized once, and almost can be used for all other lamps. This significantly reduces the deployment cost and makes RainbowLight practical.

7.6 Impact of Different Mobile Phone Models

Because different cameras have different parameters of light sensors, so they might get different hue values to the same light beam. We use the white balance algorithm to reduce the impact from different parameters of sensors, and examine the impact of different mobile phones. We use two branches of mobile phones, i.e., Huawei Nexus 6P and Vivo X7 to measure the accuracy of RainbowLight. We randomly choose 10 points in the range of z-axis between 100 and 150 cm for each mobile phone, the result is shown in Fig. 17a. We find that the error doesn't change much, so RainbowLight could be used on different mobile phone models.

7.7 Localization With Light Off

Most existing visible light positioning systems, e.g., LiTell [13], SmartLight [11], and CELLI [7], only work when the light is turned on, as those systems require modulating information in the light ray or measuring special features from the light ray. This significantly hinders their applications in the daytime when light is usually switched off. RainbowLight can work even when light is switched off during the daytime as it does not need to modulate information in light or measure light features. Fig. 17b shows the performance of RainbowLight out of 50 random points with the light turned off. Similar to Section 7.1, we examine the accuracy in the environment as shown in Fig. 13a. In the experiment, sunlight passes through the window and we switch all lamps off. We can see that the error for the light turned off is still less than 20 cm. The error for the light turned off is very small and is similar to the scenario of the light turned on. This is mainly because RainbowLight can generate obvious features from different light sources, and can also effectively extract those features. This significantly extends the application for visible light-based localization and make it more practical in everyday life.

7.8 Impact of Mobile Phone Orientation

To verify the influence of pitch and yaw, we measure error at distance 60 cm with different pitch and yaw angles.

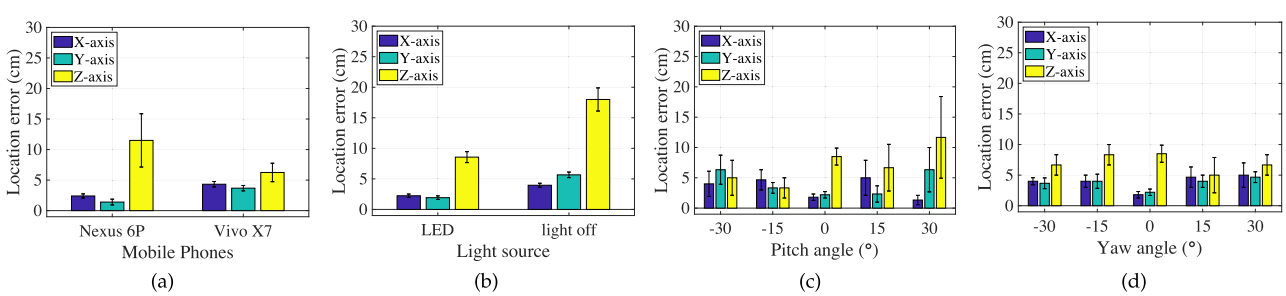

Fig. 17. Localization precision of different (a) mobile phones, (b) lamp status, (c) pitch angles of mobile phone, (d) yaw angles of mobile phone.

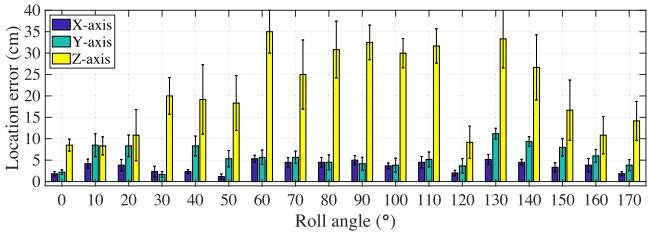

Fig. 18. Localization precision of different roll angles of camera.

Figs. 17c and 17d shows the result. We select range from -30 to 30 degree because the mobile cannot capture the lamp with pitch and yaw angle out of this range. We can see that when we change pitch and yaw angle, error changes slightly. This is mainly because when we change the pitch and yaw angle, ϕ_1, ϕ_2, γ, and θ does not change.

If P_2 is attached to the chip, mobile phone roll will have no impact on the hue value. If we put the polarizer P_2 in front of the camera, RainbowLight needs to confirm if chips on anchor show complementary hue value and its impact on localization accuracy. We also examine the accuracy of localization in this scenario. The error of different roll angles of camera as shown in Fig. 18.

Therefore, no matter which position we are, as long as we can capture the lamp with any 3D orientation, RainbowLight shows a high localization accuracy. This extends application scenarios of today's VLP systems.

8 Related Work

8.1 Visible Light Based Localization

The first category of work is to use a special designed LED light to generate identifiable features [8], [12]. Those works usually need to use an MCU to control the lamp to modulate information by change the frequency, voltage, etc. Spotlight [9] generates a sequence of on/off the pattern and uses such a pattern as landmarks for localization. Spinlight [10] uses a hemispherical shade to encode position information with holes. CELLI [7] designs a structure with LCD to modulate polarization direction of emitting light. It generates two sweeping lines with special light properties and uses sweeping lines for localization.

Recently, SmartLight [11] proposes an interesting idea to use a digital modulated LED array with a lens to achieve single light 3D localization. It modulates different LED lights with different frequency on the LED array. Then it emits the light through a lens to the 3D space. Then it derives the location based on the frequency of received light. Pulsar [21] uses the inherent features of photodiode diversity. It builds a map from angle to RSS. It designs a special receiver with two photodiodes. Most of those approaches in this category require a specially designed lamp or receiver. Thus it may not apply to most scenarios in our daily lives.

Further, many attempts are proposed to remove the requirements with specially controlled light. Existing methods such as [19], [20] use geometrical relationships among lights with the known position for triangulation based localization. PIXEL [16] leverages the inherent feature of optical rotatory dispersion for localization. When a linearly polarized light passes through a disperser, the color observed through a polarizer with different transmission directions should be different at different locations. By fixing the orientation of a mobile phone, [16] derive the identifier by the observed color, then calculates location with the geometrical relationship. It requires to capture more than one light in one photo.

LiTell [13] and iLAMP [14] use inherent features of fluorescent such as frequency and color spectrum to identify each light. Given the position of the light, the location can be derived by triangulation. Those two approaches are very nice as they do not need any extra modification to the lamp. However, they require to sample the features for each light. It is also highly related to the environment and cannot work when a lamp is changed. Recently, [29] proposes an interesting method of using light to correct inertial measurement unit errors. As introduced in [29], it leverages the property that a polarized light ray going through transparent tape is rotated by an amount related to wavelength. Then it tries to derive the location change by sensing the color after a polarizer with different directions. It detects color changes by edge crossing between four types of blocks hence serve as landmarks to correct IMU drift errors.

Luxapose [19] localizes the relative position from lamps. The main idea is to build a geometrical model and calculate the position based on the relationship between lamps' positions both in the real world and in the photo. Such a model is also used in iLAMP [14]. However, the model needs extra-parameters, e.g., focal length or data from other sensors. Since different cameras hold different parameters like the focal length, they are not easy to use. RainbowLight only uses the color pattern to derive the relative position to the tag, which is more general. Travi-Navi [30] using the computer vision-based approach to launch the navigation. It stores guider's video and uses sensors to calibrate the position, and those data can be further used for followers in navigation.

8.2 Other Localization Approaches

Localization has attracted many research efforts. Besides visible light based localization, there exist a large collection of localization approaches using wireless signal, such as [1], [2], [3], [4], [5], [6], [31], [32], [33], [34], [35], [36], using acoustic signal [37], [38], [39], using environment information and cell tower signal [40], FM signal [41], stride information [42], inertial sensors [43] etc. Those approaches are usually based on a signal attenuation model or pre-collecting a large number of fingerprints. Meanwhile, many wireless signal based approaches need to analyze signal properties such as CSI, which further leads to a high computation overhead. Thus they usually require specially designed hardware at the receiver or sender, making it difficult to implement on the mobile phone. Multiple path effect also affects the localization accuracy for many of those approaches. Our approach is largely inspired by those approaches.

9 Conclusion

We present RainbowLight, a high-precision 3D visible light based localization system. Compared with existing approaches, RainbowLight does not require special hardware design and pre-collected light features. RainbowLight works on COTS mobile phones without strict user holding requirement. It works well for different types of lamps as well as light

off scenario. Those features significantly reduce the deployment, maintenance and using overhead. The evaluation results show that RainbowLight achieves an average localization error of 3.3 cm in 2D and 9.6 cm in 3D. We believe RainbowLight can be applied to today's buildings with a very small overhead to enable many visible light based applications.

Acknowledgments

This work was supported in part by the National Key R&D Program of China 2018YFB1004800, National Natural Science Fund for Excellent Young Scholars (No. 61722210), and National Natural Science Foundation of China (No. 61572277, 61532012, 61932013, and 61432015). The preliminary version is published at ACM MobiCom 2018 and was done when Lingkun Li was a master's student at Tsinghua University under Prof. Wang. Lingkun Li and Pengjin Xie contributed equally to this work.

References

[1] S. Kumar, S. Gil, D. Katabi, and D. Rus, "Accurate indoor localization with zero start-up cost," in *Proc. 20th Annu. Int. Conf. Mobile Comput. Netw.*, 2014, pp. 483–494.
[2] F. Adib, Z. Kabelac, and D. Katabi, "Multi-person localization via rf body reflections," in *Proc. 12th USENIX Conf. Netw. Syst. Des. Implementation*, 2015, pp. 279–292.
[3] F. Adib, Z. Kabelac, D. Katabi, and R. C. Miller, "3d tracking via body radio reflections," in *Proc. 11th USENIX Conf. Netw. Syst. Des. Implementation*, 2014, pp. 317–329.
[4] M. Wang, Z. Zhang, X. Tian, and X. Wang, "Temporal correlation of the RSS improves accuracy of fingerprinting localization," in *Proc. IEEE INFOCOM*, 2016, pp. 1–9.
[5] K. Qian, C. Wu, Z. Yang, Z. Zhou, X. Wang, and Y. Liu, "Enabling phased array signal processing for mobile wifi devices," *IEEE Trans. Mobile Comput.*, vol. 17, no. 8, pp. 1820–1833, Aug. 2017.
[6] C. Duan, L. Yang, Q. Lin, and Y. Liu, "Tagspin: High accuracy spatial calibration of rfid antennas via spinning tags," *IEEE Trans. Mobile Comput.*, vol. 17, no. 10, pp. 2438–2451, Oct. 2018.
[7] Y.-L. Wei, C.-J. Huang, H.-M. Tsai, and K. C.-J. Lin, "Celli: Indoor positioning using polarized sweeping light beams," in *Proc. 15th Annu. Int. Conf. Mobile Syst. Appl. Services*, 2017, 136–147.
[8] B. Xie, K. Chen, G. Tan, M. Lu, Y. Liu, J. Wu, and T. He, "Lips: A light intensity–based positioning system for indoor environments," *ACM Trans. Sensor Netw.*, vol. 12, no. 4, 2016, Art. no. 28.
[9] R. Stoleru, T. He, J. A. Stankovic, and D. Luebke, "A high-accuracy, low-cost localization system for wireless sensor networks," in *Proc. 3rd Int. Conf. Embedded Netw. Sensor Syst.*, 2005, pp. 13–26.
[10] B. Xie, G. Tan, and T. He, "Spinlight: A high accuracy and robust light positioning system for indoor applications," in *Proc. ACM SenSys*, 2015. pp. 211–223.
[11] S. Liu and T. He, "Smartlight: Light-weight 3d indoor localization using a single led lamp," in *Proc. ACM SenSys*, 2017, pp. 1–4.
[12] N. Ravi and L. Iftode, "Fiatlux: Fingerprinting rooms using light intensity," in *Proc. Pervasive*, 2007.
[13] C. Zhang and X. Zhang, "Litell: Robust indoor localization using unmodified light fixtures," in *Proc. 22nd Annu. Int. Conf. Mobile Comput. Netw.*, 2016, pp. 230–242.
[14] S. Zhu and X. Zhang, "Enabling high-precision visible light localization in today's buildings," in *Proc. 15th Annu. Int. Conf. Mobile Syst. Appl. Services*, 2017, pp. 96–108.
[15] Q. Xu, R. Zheng, and S. Hranilovic, "Idyll: Indoor localization using inertial and light sensors on smartphones," in *Proc. ACM Int. Joint Conf. Pervasive Ubiquitous Comput.*, 2015, pp. 307–318.
[16] Z. Yang, Z. Wang, J. Zhang, C. Huang, and Q. Zhang, "Wearables can afford: Light-weight indoor positioning with visible light," in *Proc. 13th Annu. Int. Conf. Mobile Syst. Appl. Services*, 2015, pp. 317–330.
[17] M. Yoshino, S. Haruyama, and M. Nakagawa, "High-accuracy positioning system using visible led lights and image sensor," in *Proc. IEEE Radio Wireless Symp.*, 2008, pp. 439–442.
[18] S.-H. Yang, E.-M. Jeong, D.-R. Kim, H.-S. Kim, Y.-H. Son, and S.-K. Han, "Indoor three-dimensional location estimation based on led visible light communication," *Electronics Lett.*, vol. 49, no. 1, pp. 54–56, 2013.
[19] Y.-S. Kuo, P. Pannuto, K.-J. Hsiao, and P. Dutta, "Luxapose: Indoor positioning with mobile phones and visible light," in *Proc. 20th Annu. Int. Conf. Mobile Comput. Netw.*, 2014, pp. 447–458.
[20] R. Gao *et al.*, "Sextant: Towards ubiquitous indoor localization service by photo-taking of the environment," *IEEE Trans. Mobile Comput.*, vol. 15, no. 2, pp. 460–474, Feb. 2016.
[21] C. Zhang and X. Zhang, "Pulsar: Towards ubiquitous visible light localization," in *Proc. ACM MobiCom*, 2017, pp. 208–221.
[22] Z. Tian, K. Wright, and X. Zhou, "The darklight rises: Visible light communication in the dark," in *Proc. ACM MobiCom*, 2016, pp. 2–15.
[23] E. Collett, *Field Guide to Polarization*. vol. 15, Bellingham, Washington, USA: SPIE press, 2005.
[24] WikiPedia, "Birefringence," [Online]. Available: https://en.wikipedia.org/wiki/Birefringence
[25] Wikipedia, "Snell's law," [Online]. Available: https://en.wikipedia.org/wiki/Snell%27s_law
[26] S. Wei-min, "Interference pattern of convergent light for a uniaxial crystal with optical axis parallel to surface," *College Phys.*, vol. 6, 2005, Art. no. 1.
[27] D. H. Goldstein, *Polarized Light*. Boca Raton, FL, USA: CRC press, 2017.
[28] Wikipedia, "Color wheel," [Online]. Available: https://en.wikipedia.org/wiki/Color_wheel#Color_wheels_and_paint_color_mixing
[29] Z. Tian *et al.*, "Augmenting indoor inertial tracking with polarized light," in *Proc. 16th Annu. Int. Conf. Mobile Syst. Appl. Services*, 2018, pp. 362–375.
[30] Y. Zheng *et al.*, "Travi-navi: Self-deployable indoor navigation system," *IEEE/ACM Trans. Netw.*, vol. 25, no. 5, pp. 2655–2669, Oct. 2017.
[31] J. Han *et al.*, "Twins: Device-free object tracking using passive tags," *IEEE/ACM Trans. Netw.*, vol. 24, no. 3, pp. 1605–1617, Jun. 2016.
[32] J. Zhao *et al.*, "Localization of wireless sensor networks in the wild: Pursuit of ranging quality," *IEEE/ACM Trans. Netw.*, vol. 21, no. 1, pp. 311–323, Feb. 2013.
[33] K. Qian, C. Wu, Z. Yang, Y. Liu, F. He, and T. Xing, "Enabling contactless detection of moving humans with dynamic speeds using csi," *ACM Trans. Embedded Comput. Syst.*, vol. 17, no. 2, 2018, Art. no. 52.
[34] Z. Yin, C. Wu, Z. Yang, and Y. Liu, "Peer-to-peer indoor navigation using smartphones," *IEEE J. Sel. Areas Commun.*, vol. 35, no. 5, pp. 1141–1153, May 2017.
[35] K. Qian, C. Wu, Y. Zhang, G. Zhang, Z. Yang, and Y. Liu, "Widar2. 0: Passive human tracking with a single wi-fi link," *Proc. 16th Annu. Int. Conf. Mobile Syst. Appl. Services*, 2018, pp. 350–361.
[36] P. Pannuto, B. Kempke, L.-X. Chuo, D. Blaauw, and P. Dutta, "Harmonium: Ultra wideband pulse generation with band-stitched recovery for fast, accurate, and robust indoor localization," *ACM Trans. Sensor Netw.*, vol. 14, no. 2, 2018, Art. no. 11.
[37] C. Peng, G. Shen, and Y. Zhang, "Beepbeep: A high-accuracy acoustic-based system for ranging and localization using cots devices," *ACM Trans. Embedded Comput. Syst.*, vol. 11, no. 1, pp. 4:1–4:29, 2012.
[38] K. Liu, X. Liu, L. Xie, and X. Li, "Towards accurate acoustic localization on a smartphone," in *Pro. IEEE INFOCOM*, 2013, pp. 495–499.
[39] K. Liu, X. Liu, and X. Li, "Guoguo: Enabling fine-grained smartphone localization via acoustic anchors," *IEEE Trans. Mobile Comput.*, vol. 15, no. 5, pp. 1144–1156, May 2016.
[40] P. Zhou, Y. Zheng, and M. Li, "How long to wait?: Predicting bus arrival time with mobile phone based participatory sensing," in *Proc. ACM MobiSys*, 2012, pp. 379–392.
[41] Y. Chen, J. Liu, D. Lymberopoulos, and B. A. Priyantha, "Fm-based indoor localization," in *Proc. 10th Int. Conf. Mobile Syst. Appl. Services*, 2012, pp. 169–182.
[42] Y. Jiang, Z. Li, and J. Wang, "Ptrack: Enhancing the applicability of pedestrian tracking with wearables," *IEEE Trans. Mobile Comput.*, vol. 18, no. 2, pp. 431–443, Feb. 2019.
[43] R. Gao, M. Zhao, T. Ye, F. Ye, Y. Wang, and G. Luo, "Smartphone-based real time vehicle tracking in indoor parking structures," *IEEE Trans. Mobile Comput.*, vol. 16, no. 7, pp. 2023–2036, Jul. 2017.

Lingkun Li received the BE degree in software engineering from Beijing Jiaotong University and the ME degree in software engineering from Tsinghua University. He is currently working toward the PhD degree in computer science and engineering at Michigan State University. His research interests include Internet of Things and mobile computing.

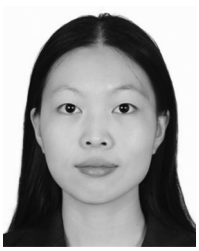

Pengjin Xie received the BE degree in Internet of Things from Chongqing University, Chongqing, China. She is currently working toward the PhD degree at Tsinghua University, Beijing, China. Her current research interests include indoor localization, Internet of Things, and mobile computing.

Jiliang Wang received the BE degree in computer science and technology from the University of Science and Technology of China, and the PhD degree in computer science and engineering from the Hong Kong University of Science and Technology. He is currently an associate professor with the School of Software and BNRist, Tsinghua University, P.R.China. His research interests include wireless and sensor networks, Internet of Things, and mobile computing. He is a member of the IEEE.